Available online at www.sciencedirect.com
ScienceDirect
Trans. Nonferrous Met. Soc. China 35(2025) 3650−3661
Transactions of Nonferrous Metals Society of China
www.tnmsc.cn

Effect of annealing process on microstructure and plane stress fracture toughness of 7075 cladding sheet

Fang YU[1], Ling-fei YANG[1], Zhong-chao ZHAO[2], Xiang-jie WANG[1], Cheng-cheng CHEN[1], Jian-zhong CUI[1]

1. Key Laboratory of Electromagnetic Processing of Materials, Ministry of Education, Northeastern University, Shenyang 110819, China;
2. Shandong Nanshan Institute of Science and Technology Co., Ltd., Longkou 265713, China

Received 5 February 2024; accepted 21 July 2024

Abstract: The effects of the inter-annealing process on the microstructure, plane stress fracture toughness, and tensile properties of an AA7075 cladding sheet were investigated using optical microscopy, scanning electron microscopy, electron backscattered diffraction, transmission electron microscopy, and mechanical property tests. The results indicate that the plane stress fracture toughness of AA7075-T6 cladding sheet can be greatly improved. The plane stress fracture toughness for the longitudinal−transverse (L−T) and transverse−longitudinal (T−L) directions were 117.7 and 94.8 MPa·m$^{1/2}$, respectively, after intermediate annealing at 380 °C. This represents an increase of 23.9 MPa·m$^{1/2}$ in the L−T direction and 22.6 MPa·m$^{1/2}$ in the T−L direction compared with the AA7075-T6 cladding sheet without intermediate annealing. Moreover, the tensile strength remains similar under different conditions. Microstructure analysis indicates that intermediate annealing before heat treatment can result in long sub-grains, few recrystallized grain boundaries, and small size precipitates in AA7075-T6 cladding sheets.

Key words: AA7075-T6 cladding sheet; intermediate annealing; plane stress fracture toughness; tensile strength; sub-grain

1 Introduction

Al−Zn−Mg−Cu alloys are widely used as aerospace structural materials due to their low density, excellent stress corrosion resistance, and fracture toughness [1,2], and 7075 cladding sheets are mainly used in aircraft skins and structural components. With the development of aviation materials, large manufacturers have increased their high damage-tolerance requirements, and now require not only the high performance of the products, but also outstanding fracture toughness and fatigue crack growth rate [3,4]. With the continuous updating and upgrading of the aerospace field, the demand for lightweight materials is also increasing, especially in terms of mass reduction in domestic large aircraft design [5−7].

To meet the requirements of the aviation industry for material performance, the development of Al−Zn−Mg−Cu alloys has gone through five stages [8,9]: (1) high strength, (2) high corrosion resistance, (3) high strength and toughness with corrosion resistance, (4) high strength, toughness, corrosion resistance and fatigue resistance, and (5) high comprehensive performance. Currently, fracture toughness is an important indicator of high-strength aluminum alloys. Only by simultaneously meeting the requirements of strength, corrosion resistance, fatigue resistance, and high fracture toughness, aluminum alloys can be considered to have high strength and excellent comprehensive performance. Therefore, high fracture toughness has become an important direction of research in high-

Corresponding author: Xiang-jie WANG, Tel: +86-24-83689561, E-mail: wangxj@epm.neu.edu.cn
https://doi.org/10.1016/S1003-6326(25)66904-4

strength aluminum alloys [10,11]. Some researchers [12] have found that the fracture toughness of the peak-aged 7050 alloy is inferior to that of the corresponding over-aged alloy, and with the extension of peak aging time, the fracture mode of the alloy transitions from transgranular fracture to intergranular fracture. CHEN et al [13] studied the fracture toughness of 7475-T7351 plates and found that the fracture morphology in the longitudinal−transverse (L−T) direction is mainly intergranular, while the proportion of transgranular fractures increases in the transverse−longitudinal (T−L) direction fracture surface. According to previous research, factors affecting plane strain fracture toughness are divided into two main categories [14]: (1) intrinsic factors, such as precipitate, matrix, precipitation free zone (PFZ), grain structure, degree of recrystallization, and constituent; and (2) extrinsic factors, such as non-metallic inclusions (Al_2O_3, refractories), metallic inclusions, and porosity. Of these factors, metallic inclusions and porosity must be controlled to as low as possible to improve facture toughness; while large constituents have detrimental effects on fracture toughness of aluminum, most studies have been mainly focused on plane strain fracture toughness [15−17].

Currently, the research on 7075 aluminum alloy around the world mainly focuses on the influence of solution and aging heat treatment systems on the microstructure and properties [18−21]. In previous studies, little work has been done on plane stress fracture toughness, especially on the plane stress fracture toughness of aluminum clad products [22−26]. However, for the industrial production of 7075-T6 aluminum cladding sheets, improving plane stress fracture toughness without reducing strength is a challenge for 7××× aluminum alloy sheets. Therefore, herein, we investigated and compared the tensile properties and plane stress fracture toughness of 3.25 mm 7075-T6-clad aluminum sheets with and without annealing heat treatment, and discussed the intrinsic relationship among the grain structure, texture, tensile properties, and fracture toughness.

2 Experimental

2.1 Materials

The experimental materials used were 7075 cold-rolled aluminum cladding sheets produced by Shandong Nanshan Aluminum Co., Ltd. The thickness of the sheet was 3.25 mm, with a 7072-cladding layer and a 7075-alloy core layer. The thickness of the 7072-cladding layer was 72 μm. The compositions of the cladding layer (7072 alloy) and the core layer (7075 alloy) are listed in Table 1. The effect of annealing temperature (280−400 °C) on the microstructure and tensile properties of the 3.25 mm-thick 7075 sheets was investigated. Additionally, samples that were annealed at 380 °C for 2 h and those in the as-rolled condition (without annealing) were selected for a solution heat treatment at 478 °C for 50 min, followed by a 121 °C, 24 h-aging treatment (7075-T6). The specific heat treatment process is shown in Table 2.

Table 1 Chemical compositions of 7075 cold-rolled aluminum clad sheet (wt.%)

Alloy	Si	Fe	Cu	Mn	Mg	Cr	Zn	Ti	Al
7072	0.04	0.12	0.02	0.08	0.04	0.001	0.98	0.03	Bal.
7075	0.04	0.10	1.40	0.01	2.45	0.20	5.70	0.05	Bal.

Table 2 Heat treatment procedures used for 7075 cold-rolled cladding sheet

Sample	Annealing process	Solution heat treatment	Aging
ST-C	−	478 °C, 50 min	121 °C, 24 h
O-280	280 °C, 2 h	−	−
O-300	300 °C, 2 h	−	−
O-320	320 °C, 2 h	−	−
O-340	340 °C, 2 h	−	−
O-360	360 °C, 2 h	−	−
O-380	380 °C, 2 h	−	−
O-400	400 °C, 2 h	−	−
ST-380	380 °C, 2 h	478 °C, 50 min	121 °C, 24 h

2.2 Mechanical property test

The plane stress fracture toughness of the 7075 cold-rolled cladding sheet was tested according to the ASTM E561 standard [27]. The size of plane stress fracture toughness sample was 750 mm × 400 mm × 3.25 mm, and center-cracked tension (CCT) specimens were used, with samples taken in the T−L and L−T directions. Plane stress fracture toughness tests were conducted on an MTS 818

testing machine, with pre-cracked fatigue cracks approximately 58 mm in length. The fracture toughness (K_C) under plane stress was calculated using the R-curve method.

Tensile properties were tested according to the ASTM E8 standard [28], using flat tensile specimens taken in the L−T direction, and the sample dimensions were 210 mm × 20 mm × 3.25 mm. Tensile tests were conducted on an Instron 8100 electronic universal testing machine, with three parallel samples for each condition.

2.3 Microstructural characterization

Qualitative analysis of the second-phase particles was performed using an energy-dispersive spectroscopy (EDS) system with SEM, and their volume fractions were measured using Image pro-Plus 6.0 analysis software. The microstructure was observed using a Tenia G2 F20 transmission electron microscope (TEM) and electron backscattered diffraction (EBSD). For TEM samples, preparation involved using an electrolyte solution of HNO_3 and methanol (1∶1 volume ratio), an electrolyte temperature of −30 °C, and a working voltage of 40 V. The electrolyte double-jet apparatus used an RL-1 electrolyte double-jet device. For EBSD samples, electrolytic polishing was carried out in a 1∶9 ethanol electrolytic polishing solution, with an electrolytic polishing voltage of 25 V and polishing time of 15 s after mechanical polishing. Data obtained from EBSD measurements were analyzed through HKL CHANNEL 5 software to obtain the grain structure of the observed area. The fracture surfaces of the specimens were analyzed using an FEI Quanta 650 field emission scanning electron microscope (SEM), with an electron beam voltage of 20 kV. The fracture surfaces were polished and etched with a liquid coating for metallographic analysis, and polarized microstructures were captured using a DM2700 Leica optical microscope.

3 Results

3.1 Microstructure

The microstructures of ST-380 and ST-C (7075-T6) are shown in Fig. 1. Comparative analysis of the longitudinal and cross-sectional microstructures of the 3.25 mm ST-C and ST-380 7075 aluminum-clad sheets showed that the

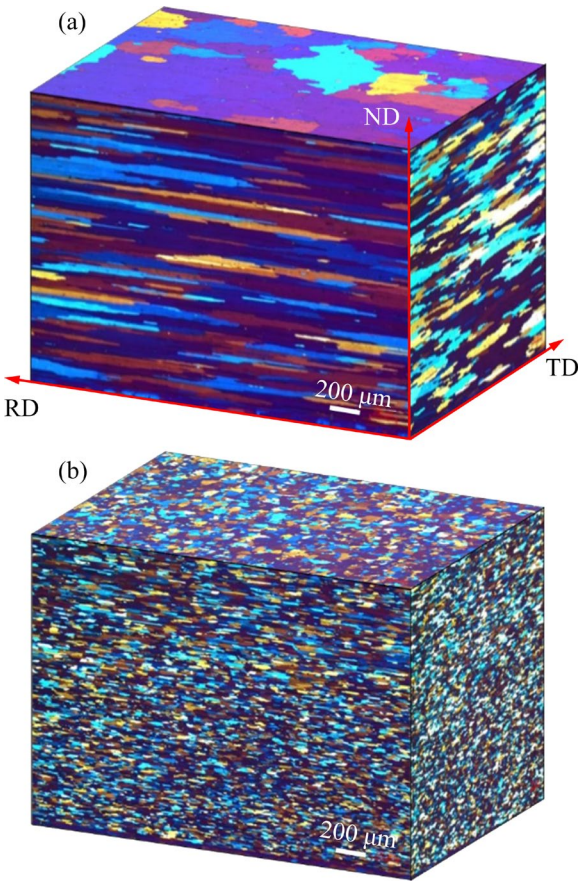

Fig. 1 Metallographic structures of 7075 aluminum-clad sheets: (a) ST-380; (b) ST-C

recrystallization degree of the ST-380 sample was lower than that of the ST-C sample. Many original deformed grains remained in ST-380 sample, and many fine substructures could be found inside these grains. Figure 2 shows the EBSD image of the 7075-T6 aluminum-clad sheet, which underwent recrystallization regardless of whether it had been annealed or not, while the ratio of the sub-grain boundary differed significantly between samples annealed at 380 °C, being 15.4% and 4% for ST-C samples without annealing process. The grain sizes of the ST-380 and ST-C samples are shown in Table 3. After annealing, the grain size of the surface layer of ST-380 was 283.46 μm, which was 8.16 times that of the ST-C samples. The transverse grain size of ST-380 was 42.48 μm, which was 1.7 times that of the sample without annealing, and the aspect ratio of the grains also decreased by 64.3%. The deformation energy storage decreased after annealing, which led to grain coarsening and fusion during the subsequent solution treatment.

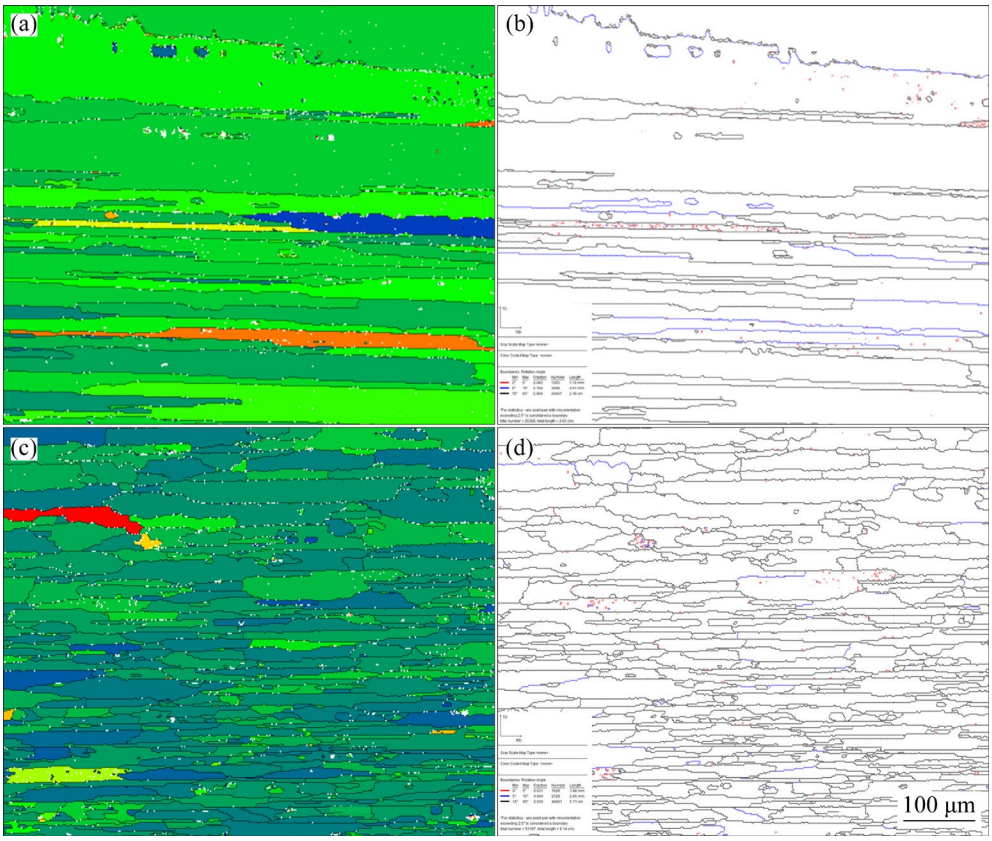

Fig. 2 Recrystallization microstructure (GOS) (a, c) and grain boundary (b, d) in longitude-short plane of 7075 cladding sheet: (a, b) ST-380; (c, d) ST-C

Table 3 Grain size of 7075 aluminum-clad sheet

Sample	Grain size/μm		Aspect ratio/%
	Surface	Transverse	
ST-380	283.5±7.5	42.5±2.3	5.57
ST-C	34.8±1.8	24.9±1.5	3.39

After heat solution and aging treatment, the main second phase mainly consisted of Al_7Cu_2Fe (Fig. 3) for both ST-380 and ST-C samples. And there have not much difference for the morphology of the second phase. After statistical analysis, the second phase ratio for ST-380 samples was 0.55%, while it was 0.52% for ST-C samples. Therefore, although ST-380 underwent annealing before the heat solution treatment, the amount and morphology of the second phase was similar between samples.

The orientation distribution function sections of φ_2 mm from 0° to 90° (with an interval of 5°) for two different processes are shown in Figs. 4(a, b). For the 7075-T6 samples, the intermediate annealing process resulted in no noticeable difference in the texture component; the main texture component of the sheets included (001)⟨100⟩ Cube, (001)⟨110⟩ Cube, (132)⟨$6\bar{4}3$⟩ S, and (123)⟨$41\bar{2}$⟩ R textures, as well as small amounts of (110)⟨001⟩ Goss, (110)⟨$1\,\bar{1}2$⟩ Brass, and (112)⟨$11\,\bar{1}$⟩ Copper textures. The volume fractions of main textures are shown in Fig. 4(c). For ST-C samples, the proportion of Cube texture (⟨100⟩ Cube and ⟨110⟩ Cube) was 21.38%, while for ST-380, the proportion of Cube texture was 16.92%. The proportions of the Brass, S, and R textures for ST-380 were 4.5%, 2.43%, and 2.78%, respectively, compared with 2.2%, 2.05%, and 2.08% for the ST-C samples. The fraction of Cube component textures for ST-C was higher than that for ST-380, indicating that ST-C had a more recrystallized microstructure, which is consistent with the result shown in Fig. 2.

3.2 Mechanical properties

The effect of annealing temperature on tensile properties is illustrated in Fig. 5, which shows that as the annealing temperature increased to 340 °C, the strength of the 7075 cladding sheets decreased significantly (the tensile strength decreased from

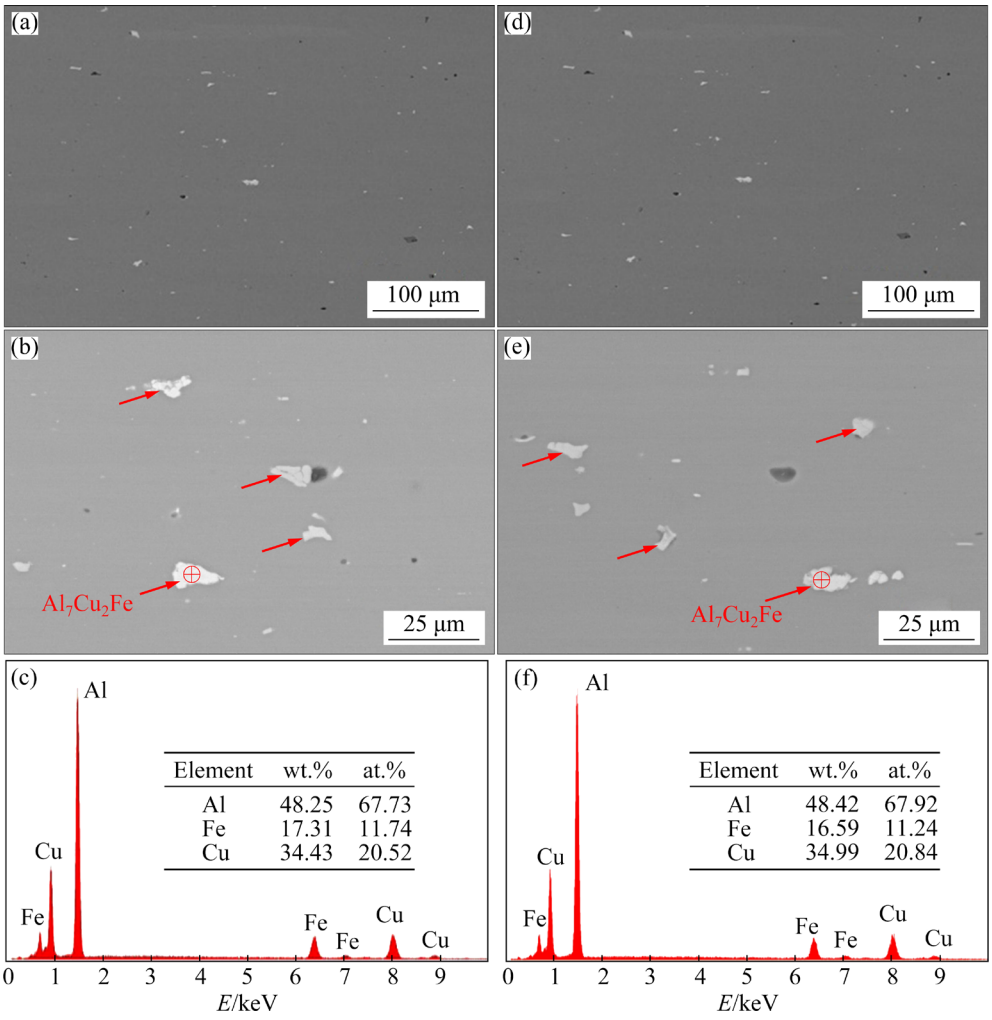

Fig. 3 SEM images (a, b, d, e) and EDS analysis results (c, f) of composite sheets after different treatments: (a, b, c) ST-380; (d, e, f) ST-C

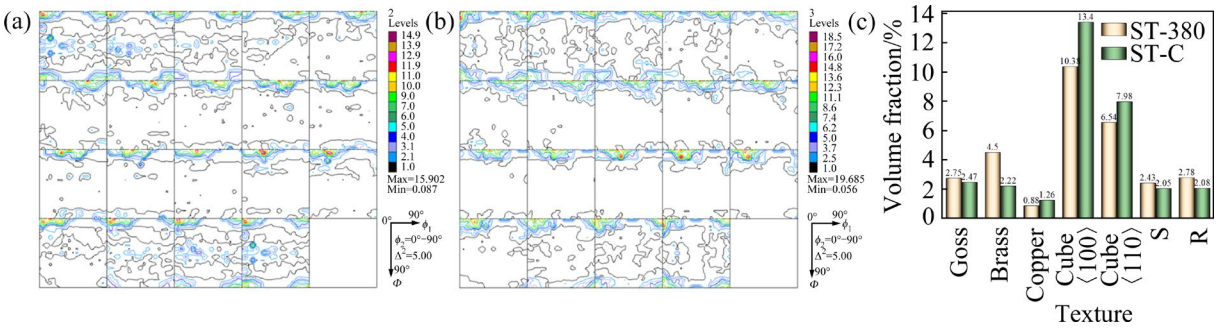

Fig. 4 ODF maps of 7075 cladding sheets with different treatments: (a) ST-380; (b) ST-C; (c) Volume fraction of main texture components

275 to 225 MPa, while the yield strength decreased from 226 to 100 MPa) and the elongation increased. The elongation was 12.5% after annealing at 280 °C, and it increased to 19% when annealed at 340 °C. When the annealing temperature was greater than 360 °C, the tensile properties of the 7075 aluminum-clad sheets tended to stabilize.

The plane stress fracture toughness results of a 3.25 mm 7075-clad aluminum sheet after 2 h of annealing at 380 °C and subsequent solution treatment (ST-380), compared with the same sheet after direct solution treatment and aging heat treatment (ST-C), are shown in Table 4. Figure 6 shows the K_R curves (K_R vs Δa_e) obtained from the

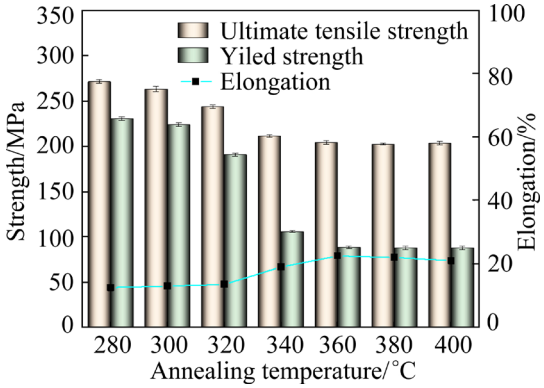

Fig. 5 Effect of annealing temperature on tensile properties

CCT samples. Table 4 indicates that the plane stress fracture toughness K_C in the L−T direction for the ST-C sample was 93.8 MPa·m$^{1/2}$, while in the T−L direction, it was 72.2 MPa·m$^{1/2}$, with the K_C in the L−T direction being 21.6 MPa·m$^{1/2}$ higher than that in the T−L direction. After intermediate annealing at 380 °C, the plane stress fracture toughness K_C in the L−T and T−L directions for 7075-T6 cladding sheets were 117.7 and 94.8 MPa·m$^{1/2}$, respectively.

Table 4 7075 aluminum-clad plane stress fracture toughness

Sample	K_C/(MPa·m$^{1/2}$)		Yield stress (L−T)/MPa
	L−T	T−L	
ST-380	117.7	94.8	481±2.3
ST-C	93.8	72.2	480±2.8

Compared with ST-C (7075-T6 cladding sheets without annealing), the plane stress fracture toughness K_C in the L−T direction for ST-380 increased by 23.9 MPa·m$^{1/2}$, and in the T−L direction, it increased by 22.6 MPa·m$^{1/2}$, meanwhile, the yield stress for both the ST-380 and ST-C samples remained similar.

3.3 Fractography

The plane stress fracture surfaces of the ST-380 and ST-C samples are shown in Fig. 7. From Figs. 7(a) and (c), in the early stage of crack propagation (near the pre-crack area), both fracture modes in the ST-380 and ST-C states show a combination of transgranular and intergranular fractures. Compared with samples without intermediate

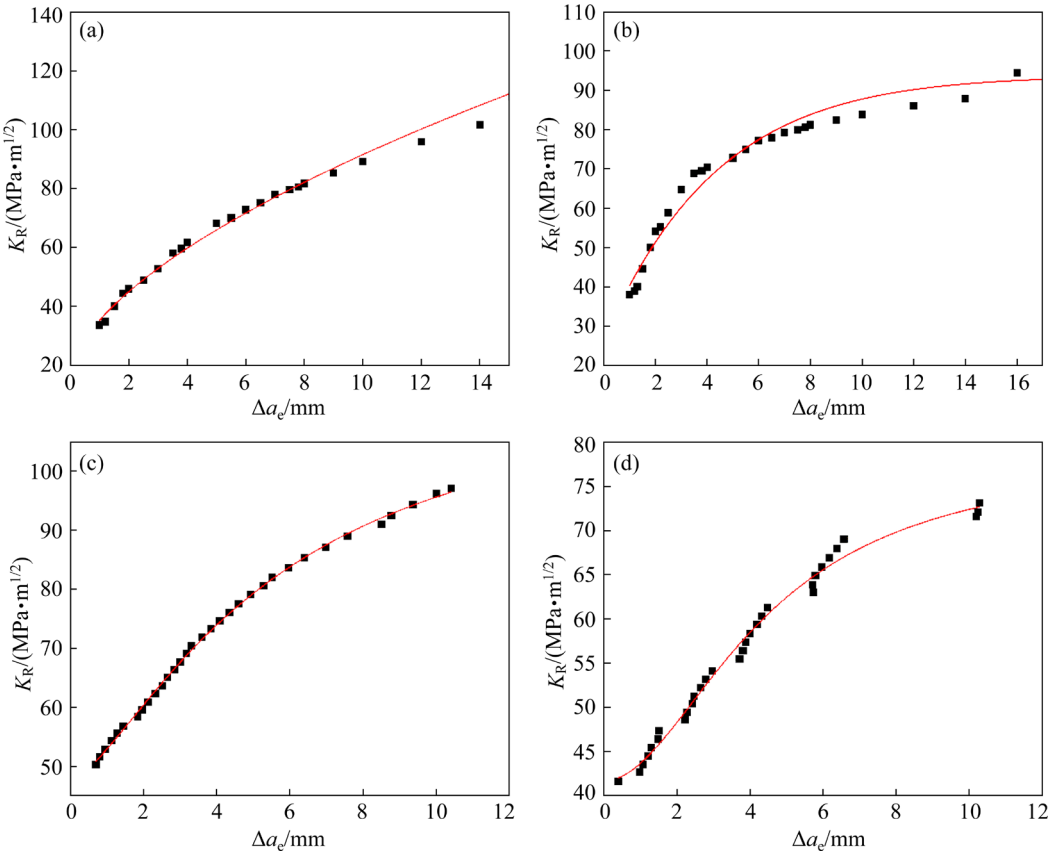

Fig. 6 K_R−Δa_e curves for 7075-T6 cladding sheet: (a) ST-380 in L−T direction; (b) ST-380 in T−L direction; (c) ST-C in L−T direction; (d) ST-C in T−L direction (K_R: Crack growth resistance; Δa_e: Crack growth increment)

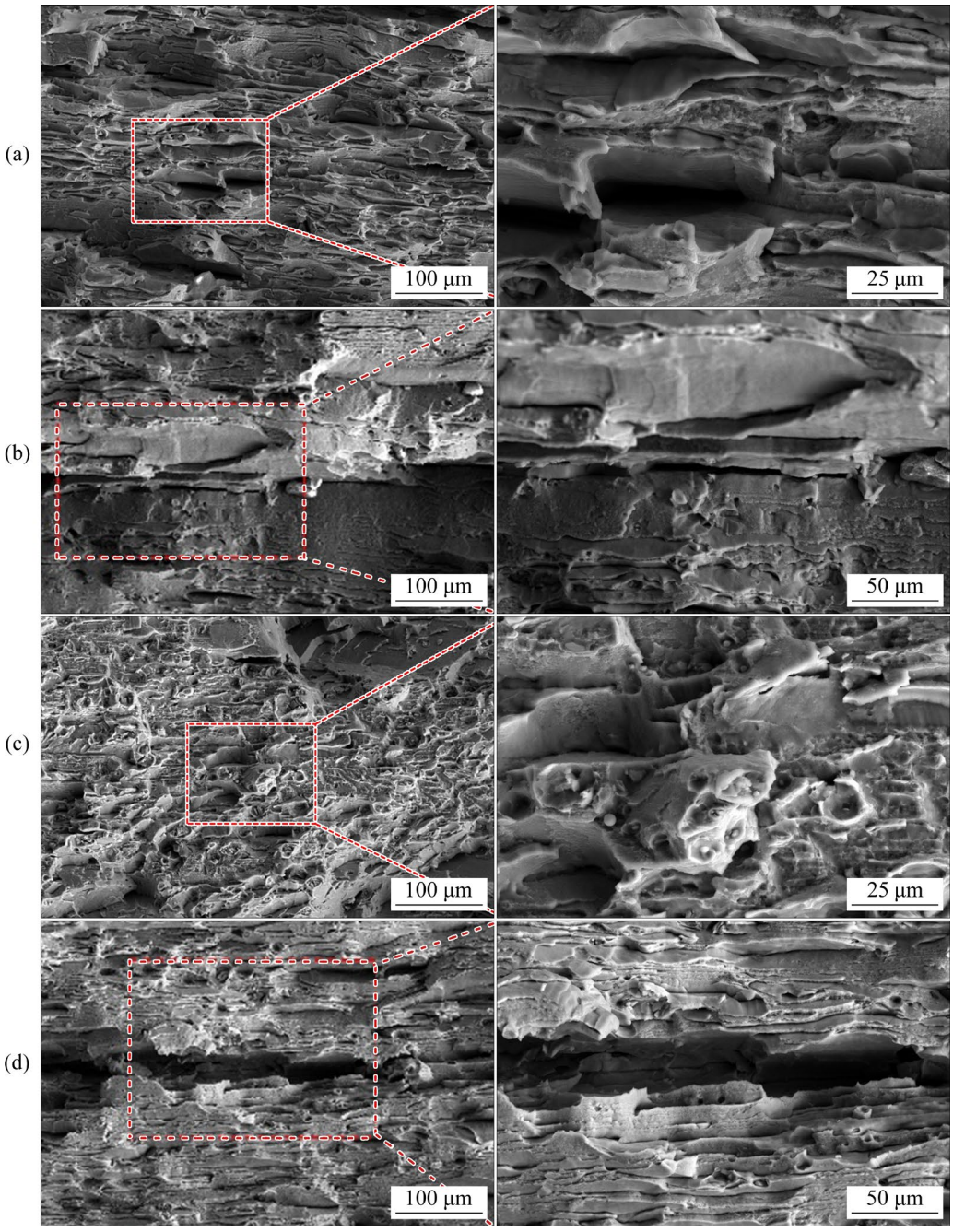

Fig. 7 Fracture surface of 7075 cladding sheet under different temper conditions in early (a, c) and late (b, d) stages of crack propagation: (a, b) ST-C; (c, d) ST-380

annealing, the ratio of intergranular fracture for ST-C samples was higher, and the cleavage fracture characteristics were observed in local areas, with smaller number and dimple sizes on the fracture plane, as well as a flatter transgranular plane. The ST-380 samples showed more dimples, with the second phase found within the dimples. In the late stage of crack propagation (Figs. 7(b) and (d)), the fracture surface of ST-380 samples exhibited more layered features, with some uneven dimples around the tearing edges, when the crack propagated under stress into these layered structures, crack propagation could be hindered, thereby improving the fracture toughness of the samples. In contrast, the fracture surface of ST-C samples appeared smoother and flatter, and the proportion of transgranular fractures of the ST-C samples were lower, exhibiting more intergranular fractures. The intergranular fractures mainly occurred at high-angle grain boundaries, consistent with the EBSD results in Fig. 2. Therefore, the ST-380 samples exhibited high fracture toughness.

4 Discussion

4.1 Effects of microstructure on fracture toughness

The fracture toughness of thin materials under plan stress conditions is significantly affected by the grain structure, subgrain boundaries, and recrystallized grain boundaries. According to ASTM E561 [27], for CCT specimens, the crack growth resistance (K_R) can be calculated as follows:

$$K_R = \frac{P}{WB} \cdot \sqrt{\frac{\pi a}{\cos\left(\frac{\pi a}{W}\right)}} \quad (1)$$

where P, W, B and a are the maximum applied load, sample width (400 mm), sample thickness (3.25 mm), and crack size, respectively. Therefore, the main factors effecting plane stress fracture are maximum applied max load and crack size, which mainly depend on the strength difference between the matrix and grain boundaries [16]. These factors are closely related to the grain structure, the size and quantity of matrix and grain boundary precipitates, and the width of the precipitate-free zone [29−32]. As observed in the TEM images (Fig. 8), there was no significant difference in the width of the precipitation-free zone and the size of precipitates at different conditions of 7075 aluminum sheets, while the size of precipitates at the grain boundaries for ST-C was larger than that in ST-380, which could potentially lead to stress concentration points.

The grain size and degree of recrystallization have significant effects on fracture toughness. The degree of recrystallization depends on the thickness of the product, as well as whether it is under plane stress or plane strain conditions [15]. In sheet products under plane stress, fracture toughness is primarily controlled by plasticity. Therefore, in this case it is preferable for the recrystallized grain size to be small. If the grain size is sufficiently small, plasticity will be enhanced and harmful, low-energy, intergranular fracture modes will be avoided [33,34]. In addition, as shown in Fig. 2, the proportions of high-angle grain boundaries in the 7075 aluminum-clad sheets in the ST-380 and ST-C states are 80.6% and 93%, respectively. Small-angle grain boundaries have an inhibitory effect on crack propagation, whereas high-angle grain boundaries accelerate crack propagation, especially when large precipitates are formed along them during quenching and aging processes, which can easily lead to intergranular fracture. The more the high-angle grain boundaries are, the higher the crack propagation rate and the lower the fracture toughness will be. After annealing, the grain morphology of ST-380 was elongated, while that of

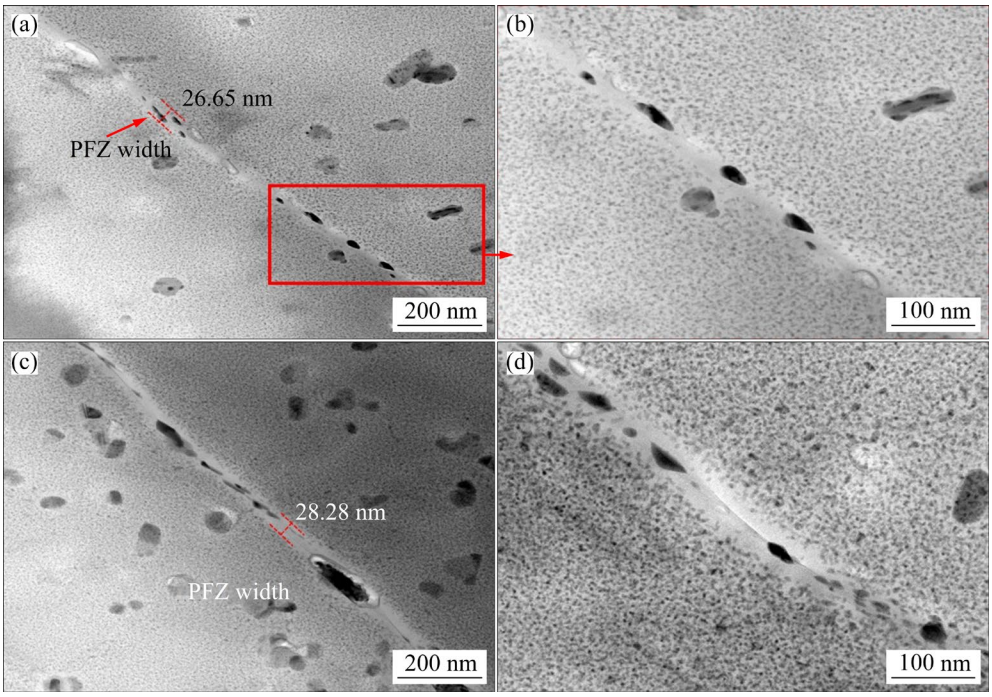

Fig. 8 TEM images of 7075-T6 aluminum-clad sheet in different states: (a, b) ST-380; (c, d) ST-C

ST-C was equiaxed. Figure 9 shows the effect of grain structure on the fracture toughness of aluminum alloys at different thicknesses [35]. Typically, deformed fibrous grains have the highest fracture toughness, followed by subgrains, and a completely recrystallized microstructure has the worst fracture toughness. Therefore, the degree of subgrain structure affects the plane stress fracture toughness. Research on the influence of the grain morphology of recrystallized microstructures on fracture toughness has shown that elongated recrystallized microstructures have the best fracture toughness, followed by general recrystallized microstructures, and finally by equiaxed fine grain microstructures, which have the worst toughness [36]. Subsequent test results for fracture toughness K_C in Table 4 also confirm this finding. After recrystallization, the fracture toughness of the elongated grain structure is higher than that of the equiaxed fine grain structure [1,3,14,37]. Therefore, the presence of long sub-grains, few large grain boundaries and small precipitates improves the fracture toughness of 7075 cladding sheets.

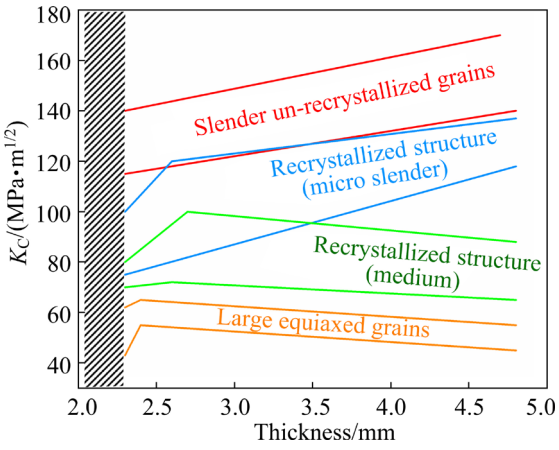

Fig. 9 Relationship between various grain structures and fracture toughness of aluminum alloys at different thicknesses

4.2 Crack propagation mechanism in rolled AA7075 cladding sheet

For ST-C samples, the presence of fine equiaxed grains facilitates crack propagation along grain boundaries. In contrast, in ST-380 samples, the energy required for crack deflection or bridging across elongated grains is much higher. In fact, when the crack is perpendicular to the main axis of the grain, the elongated grain morphology hinders crack propagation. In these cases, the proportion of transgranular fracture increases, resulting in higher energy absorption and an increase in K_C value to higher levels, which is consistent with the fractographic results in Fig. 7. Therefore, there is a competitive effect of microstructure on crack initiation and propagation [34,37]. The toughness of 7xxx aluminum alloys is closely related to a change in the fracture mechanism, where a higher proportion of intergranular fracture leads to shorter crack propagation paths and a lower toughness of the material [38,39]. The low fracture toughness observed in the ST-C condition alloys was attributed to a change in the crack propagation mechanism, cracks easily propagated along the grains in the ST-C condition alloys, and intergranular fracture covered a significant portion of the propagation surfaces (Fig. 10(a)). In contrast, as clearly observed in the fracture patterns of the ST-380 sample in Figs. 7(c, d) the ST-380 sample exhibited a mixed propagation mode of intergranular and transgranular fractures. In addition, in the crack propagation sample, the presence of a sharp crack tip enhances the triaxial stress state and leads to a significant deviation from the nominal stress. This deviation increases the resistance to crack propagation. If the crack direction is perpendicular to the grains, the presence of elongated rolled grains helps delay crack propagation (Fig. 10(b)). An investigation of WANG et al [40] also confirmed the trend of crack propagation in recrystallized grains in rolled materials.

5 Conclusions

(1) The tensile properties of AA7075 cladding sheet decreased significantly at an elevated annealing temperature and tended to stabilize when the annealing temperature was greater than 360 °C.

(2) Compared with samples without annealing, the AA7075-T6 plane stress fracture toughness value (K_C) with an intermediate annealing process showed excellent fracture toughness in both L−T and T−L directions, with K_C values of 117.7 and 94.8 MPa m$^{1/2}$, respectively.

(3) An intermediate annealing process has a significant effect on the grain structure of AA7075-T6 cladding sheets. After annealing, the AA 7075-T6 samples had more sub-grain boundaries, with a proportion of 15.4%, compared with 4% in ST-C sample without annealing.

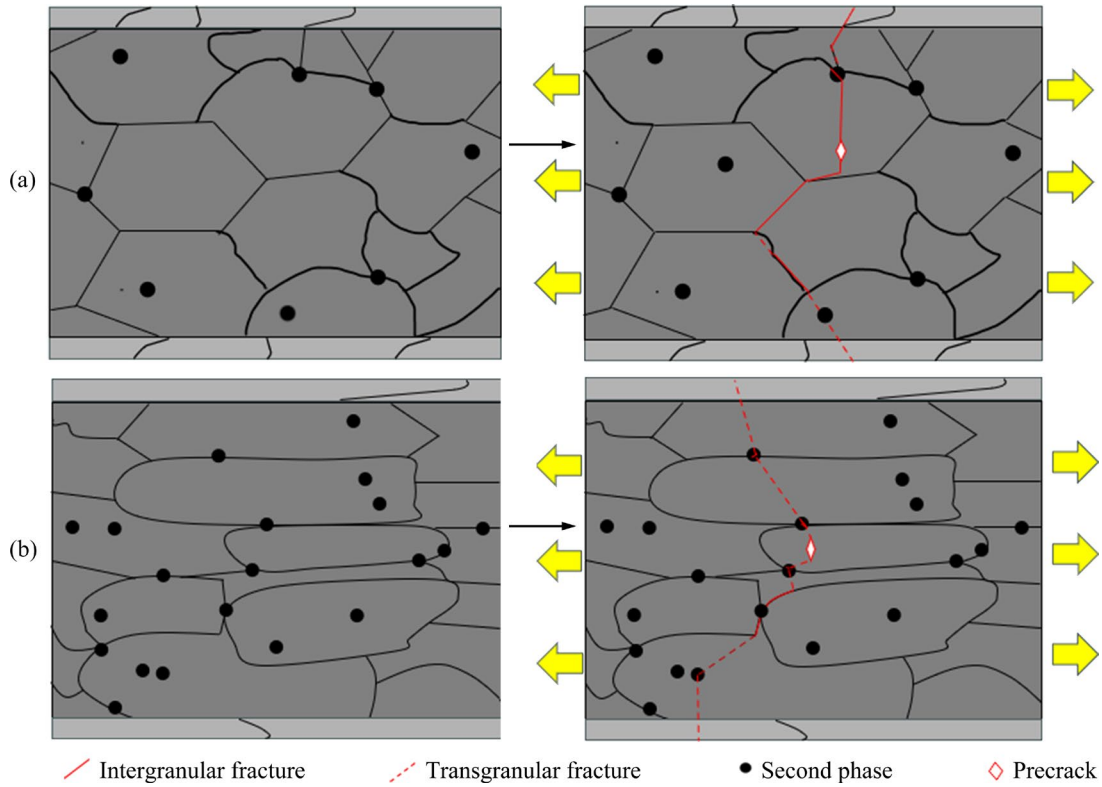

Fig. 10 Recrystallization structure crack propagation mechanism diagram: (a) Equiaxed grain structure without intermediate annealing; (b) Elongated grain structure with intermediate annealing

(4) Fracture analysis showed that the fracture surface of the alloy in the ST-380 state exhibited more layered features, with some uneven dimples around the tearing edges. In contrast, the fracture surface of the alloy in the ST-C state appeared both smoother and flatter.

(5) A long sub-grain size, low number of large grain boundaries and small precipitate size are beneficial for the plane stress fracture toughness of AA7075 cladding sheets.

CRediT authorship contribution statement

Fang YU: Conceptualization, Formal analysis, Methodology & experimental design, Writing − Review & editing; **Ling-fei YANG:** Software, Data curation, Investigation; **Zhong-chao ZHAO:** Writing − Original draft, Investigation; **Xiang-jie WANG:** Funding acquisition, Supervision; **Cheng-cheng CHEN:** Investigation; **Jian-zhong CUI:** Resources, Funding acquisition.

Declaration of competing interest

The authors declare that they have no known competing financial interests or personal relationships that could have appeared to influence the work reported in this paper.

Acknowledgments

The authors would like to thank the National Key R&D Program of China (Nos. 2023YFB3710401, 2022YFB3504401), the National Natural Science Foundation of China (Nos. 52271094, U1708251), the Key Research and Development Program of Liaoning, China (No. 2020JH2/10700003), and Qingyuan City Science and Technology Plan Project (No. 2023YFJH003), China.

References

[1] HEINZ A, HASZLER A, KEIDEL C, MOLDENHAUER S, BENEDICTUS R, MILLER W S. Recent development in aluminium alloys for aerospace applications [J]. Materials Science and Engineering: A, 2000, 280: 102−107.

[2] ZHANG Xue-song, CHEN Yong-jun, HU Jun-ling. Recent advances in the development of aerospace materials [J]. Progress in Aerospace Sciences, 2018, 97: 22−34.

[3] LEZAACK M B, HANNARD F, SIMAR A. Understanding the ductility versus toughness and bendability decoupling of large elongated and fine grained Al 7475-T6 alloy [J]. Materials Science and Engineering: A, 2022, 839: 142816.

[4] LI Qiang, HUANG Sheng, ZHAO Ya-kai, GAO Yi-min, RAMAMURTY U. Simultaneous enhancements of strength, ductility, and toughness in a TiB reinforced titanium matrix composite [J]. Acta Materialia, 2023, 254: 118995.

[5] LIU Bing, PENG Chao-qun, WANG Ri-chu, WANG

Xiao-feng, LI Ting-ting. Recent development and prospects for giant plane aluminum alloys [J]. The Chinese Journal of Nonferrous Metals, 2010, 20: 1705−1715. (in Chinese)

[6] DENG Yun-lai, ZHANG Xin-ming. Development of aluminum and aluminum alloy [J]. The Chinese Journal of Nonferrous Metals, 2019, 29: 2116−2141. (in Chinese)

[7] WILLIAMS J C, STARKE E A Jr. Progress in structural materials for aerospace systems [J]. Acta Materialia, 2003, 19: 5775−5799.

[8] LI Shuang-shuang, YUE Xin, LI Qiang-yuan, PENG He-li, DONG Bai-xin, LIU Tian-shu, YANG Hong-yu, FAN Jun, SHU Li-shi, QIU Feng, JIANG Qi-chuan. Development and applications of aluminum alloys for aerospace industry [J]. Journal of Materials Research and Technology, 2023, 67: 944−983.

[9] JUAN Yong-fei, NIU Guo-shuai, YANG Yang, XU Zi-han, YANG Jian, TANG Wen-qi, JIANG Hai-tao, HAN Yan-feng, DAI Yong-bing, ZHANG Jiao, SUN Bao-de. Accelerated design of Al−Zn−Mg−Cu alloys via machine learning [J]. Transactions of Nonferrous Metals Society of China, 2024, 34: 709−723.

[10] LAI M O, FERGUSON W G. Fracture toughness of aluminium alloy 7075-T6 in the as-cast condition [J]. Materials Science and Engineering, 1985, 74: 133−138.

[11] PETIT T, BESSON J, RITTER C, COLAS K, HELFEN L, MORGENEYER T F. Effect of hardening on toughness captured by stress-based damage nucleation in 6061 aluminum alloy [J]. Acta Materialia, 2019, 180: 349−365.

[12] HAN Nian-mei, ZHANG Xin-ming, LIU Sheng-dan, KE Bin, XIN Xing. Effects of pre-stretching and ageing on the strength and fracture toughness of aluminum alloy 7050 [J]. Materials Science and Engineering: A, 2011, 528: 3714−3721.

[13] CHEN Jun, DUAN Yu-lu, PENG Xiao-yan, CAO Xiao-wu, XU Guo-fu, YIN Zhi-min. Fracture toughness of 7475-T7351 aluminum alloy thick plate [J]. Journal of Central South University, 2015, 46: 437−443. (in Chinese)

[14] STARKE E A, STALEY J T. Application of modern aluminum alloys to aircraft [J]. Progress in Aerospace Sciences, 1996, 32: 747−783.

[15] DUMONT D, DESCHAMPS A, BRECHET Y. On the relationship between microstructure, strength and toughness in AA7050 aluminum alloy [J]. Materials Science and Engineering A, 2003, 356: 326−336.

[16] CHEN Song-yi, CHEN Kang-hua, DONG Peng-xuan, YE Sheng-ping, HUANG Lan-ping. Effect of heat treatment on stress corrosion cracking, fracture toughness and strength of 7085 aluminum alloy [J]. Transactions of Nonferrous Metals Society of China, 2014, 24: 2320−2325.

[17] CHEN Gao-hong, LI Guo-ai, CHEN Jun-zhou, RU Ji-gang, HE Wei-wei. Effect of rolling microstructure characteristics on fracture toughness of 7B50-T7751 aluminum alloy thick plate [J]. Light Alloy Fabrication Technology, 2018, 46(6): 29−33. (in Chinese)

[18] CEPEDA-JIMÉNEZ C M, POZUELO M, RUANO O A, CARREÑO F. Influence of the thermal treatment on the microstructure and hardness evolution of 7075 aluminium layers in a hot-rolled multilayer laminate composite [J]. Journal of Alloys and Compounds, 2009, 478: 154−162.

[19] MO Tian-qian, CHEN Ze-jun, ZHOU Zhan-song, LIU Jiang-jiang, HE Wei-jun, LIU Qing. Enhancing of mechanical properties of rolled 1100/7075 Al alloys laminated metal composite by thermomechanical treatments [J]. Materials Science and Engineering: A, 2021, 800: 140313.

[20] HUO Wang-tu, SUN Tao-tao, HOU Long-gang, ZHANG Wei, ZHANG Yu-sheng, ZHAN Ji-shan. Effect of heating rate during solution treatment on microstructure, mechanical property and corrosion resistance of high-strength AA 7075 alloy [J]. Materials Characterization, 2020, 167: 110535.

[21] WU Fan, ZHOU Wen-long, ZHAO Bing, HOU Hong-liang. Interface microstructure and bond strength of 1420/7B04 composite sheets prepared by diffusion bonding [J]. Rare Metals, 2018, 37: 613−620.

[22] DODDAMANI S, KALEEMULLA M. Review of experimental fracture toughness (KIC) of aluminium alloy and aluminium MMCs [J]. International Journal of Fracture and Damage Mechanics, 2015, 1: 1−15.

[23] LUDTKA G M, LAUGHLIN D E. The influence of microstructure and strength on the fracture mode and toughness of 7xxx series aluminum alloys [J]. Metallurgical Transactions A, 1982, 13: 411−425.

[24] DESHPANDE N U, GOKHALE A M, DENZER D K, LIU J. Relationship between fracture toughness, fracture path, and microstructure of 7050 aluminum alloy: Part I. Quantitative characterization [J]. Metallurgical and Materials Transactions A, 1998, 29: 1191−1201.

[25] SHIH T S, HSU H T, HWANG L R. Factors affecting the microstructure, tensile properties and corrosion resistance of AA7075 forgings [J]. Materials, 2021, 14: 5776.

[26] BHUIYAN M S, TODA H, SHIMIZU K, SU H, UESUGI K, TAKEUCHI A, WATANABE Y. The role of hydrogen on the local fracture toughness properties of 7xxx aluminum alloys [J]. Metallurgical and Materials Transactions A, 2018, 49: 5368−5381.

[27] ASTM E561—2023. Standard test method for KR curve determination [S].

[28] ASTM E8M—2022. Standard test methods for tension testing of metallic materials [S].

[29] GOKHALE A M, DESHPANDE N U, DENZER D K, LIU J. Relationship between fracture toughness, fracture path, and microstructure of 7050 aluminum alloy: Part II. Multiple micromechanisms-based fracture toughness model [J]. Metallurgical and Materials Transactions A, 1998, 29: 1203−1210.

[30] CVIJOVIĆ Z, RAKIN M, VRATNICA M, CVIJOVI Ć I. Microstructural dependence of fracture toughness in high-strength 7000 forging alloys [J]. Engineering Fracture Mechanics, 2008, 75: 2115−2129.

[31] CVIJOVIĆ Z, VRATNICA M, RAKIN M. Micromechanical modelling of fracture toughness in overaged 7000 alloy forgings [J]. Materials Science and Engineering: A, 2006, 434: 339−346.

[32] HAHN G T, ROSENFIELD A R. Metallurgical factors affecting fracture toughness of aluminum alloys [J]. Metallurgical Transactions A, 1975, 6: 653−668.

[33] LIU Sheng-dan, LI Qun, LIN Hua-qiang, SUN Lin, LONG

Tao, YE Ling-ping, DENG Yun-lai. Effect of quench-induced precipitation on microstructure and mechanical properties of 7085 aluminum alloy [J]. Materials & Design, 2017, 132: 119−128.

[34] LEZAACK M B, HANNARD F, ZHAO L, OREKHOV A, ADRIEN J, MIETTINEN A, IDRISSI H, SIMAR A. Towards ductilization of high strength 7xxx aluminium alloys via microstructural modifications obtained by friction stir processing and heat treatments [J]. Materialia, 2021, 20: 101248.

[35] PAN Zhi-jun, LI Wen-xian. Current status and future trends of research on fracture toughness of high strength aluminum alloys [J]. Material Review, 2007, 16: 14−17.

[36] DUMONT D, DESCHAMPS A, BRECHET Y. A model for predicting fracture mode and toughness in 7000 series aluminium alloys [J]. Acta Materialia, 2004, 52: 2529−2540.

[37] TAJALLY M, EMADODDIN E. Mechanical and anisotropic behaviors of 7075 aluminum alloy sheets [J]. Materials & Design, 2011, 32: 1594−1599.

[38] MORERE B, EHRSTRÖM J C, GREGSON P J, SINCLAIR I. Microstructural effects on fracture toughness in AA7010 plate [J]. Metallurgical and Materials Transactions A, 2000, 31: 2503−2515.

[39] HANNARD F, SIMAR A, MAIRE E, PARDOEN T. Quantitative assessment of the impact of second phase particle arrangement on damage and fracture anisotropy [J]. Acta Materialia, 2018, 148: 456−466.

[40] WANG Yi-chang, WU Xiao-dong, CAO Ling-fei, TONG Xin, COUPER M J, LIU Qing. Effect of trace Er on the microstructure and properties of Al−Zn−Mg−Cu−Zr alloys during heat treatments [J]. Materials Science and Engineering: A, 2020, 792: 139807.

退火工艺对 7075 复合薄板组织和平面应力断裂韧性的影响

于 芳[1]，杨凌飞[1]，赵忠超[2]，王向杰[1]，陈诚诚[1]，崔建忠[1]

1. 东北大学 材料电磁过程研究教育部重点实验室，沈阳 110819；
2. 山东南山科学技术研究院，龙口 265713

摘 要：通过光学显微镜、扫描电子显微镜、电子背散射衍射和透射电子显微镜及力学性能测试，研究中间退火对 AA7075 复合薄板显微组织、平面应力断裂韧性及拉伸性能的影响。结果表明，AA7075-T6 复合薄板的平面应力断裂韧性可显著提高，经过 380 ℃中间退火后，纵向−横向(L−T)方向的断裂韧性为 117.7 MPa·$m^{1/2}$，纵向−横向(T−L)方向的断裂韧性为 94.8 MPa·$m^{1/2}$，与未进行中间退火的 AA7075-T6 复合薄板相比，中间退火后 L−T 和 T−L 方向的断裂韧性分别提高了 23.9 和 22.6 MPa·$m^{1/2}$，此外，在不同条件下，拉伸强度无明显差异。显微组织分析表明，在热处理前中间退火导致 AA 7075-T6 薄板组织中形成更长的亚晶粒、少量再结晶晶界及小尺寸的析出相。

关键词：AA7075-T6 复合薄板；中间退火；平面应力断裂韧性；拉伸强度；亚晶粒

(Edited by Xiang-qun LI)